An endstation for resonant inelastic X-ray scattering studies of solid and liquid samples

Zhong Yin,[a,b] Hans-Bernhard Peters,[a] Ulrich Hahn,[a] Josef Gonschior,[a] Daniel Mierwaldt,[c] Ivan Rajkovic,[b] Jens Viefhaus,[a] Christian Jooss[c] and Simone Techert[a,b,d]*

[a]Photon Science, Deutsches Elektronen-Synchrotron, Notkestrasse 85, 22607 Hamburg, Germany, [b]Structural Dynamics of (Bio)chemical Systems, Max Planck Institute for Biophysical Chemistry, Am Fassberg 11, 37077 Goettingen, Germany, [c]Institute for Material Physics, University of Goettingen, Friedrich-Hund-Platz 1, 37077 Goettingen, Germany, and [d]Institute for X-ray Physics, University of Goettingen, Friedrich-Hund Platz 1, Goettingen, Germany. *Correspondence e-mail: simone.techert@desy.de

A novel experimental setup is presented for resonant inelastic X-ray scattering investigations of solid and liquid samples in the soft X-ray region for studying the complex electronic configuration of (bio)chemical systems. The uniqueness of the apparatus is its high flexibility combined with optimal energy resolution and energy range ratio. The apparatus enables investigation of chemical analyses, which reflects the chemical imprints. The endstation is composed of a main sample chamber, a sample holder for either solid or liquid jet delivery system, and a soft X-ray grating spectrometer for 210–1250 eV with a resolving power of ~1000. It combines for the first time liquid jet technology with a soft X-ray spectrometer based on the variable line spacing principle. This setup was commissioned at the soft X-ray beamline P04 at PETRA III of the Deutsches Elektronen-Synchrotron in Hamburg which is currently the most brilliant storage-ring-based X-ray radiation source in the world. The first results of liquid and solid samples show that this setup allows the detection of photons across an energy range of ~300 eV. This covers simultaneously the emission lines of life-important elements like carbon, nitrogen and oxygen in a shot-based procedure.

1. Introduction

Chemical reactions are governed by the properties of the electronic structure. Information about the electronic configuration reveals the chemical pathways of these reactions. Soft X-ray spectroscopy is a powerful method of studying the occupied and unoccupied molecular orbitals of systems with low detection efficiency (Ament *et al.*, 2011; Kotani & Shin, 2001). It has become an established method at modern light sources such as synchrotron radiation or free-electron laser facilities due to their continuous improvement and development which has led to a remarkable increase in brilliance, coherence and short pulse width compared with previous light source facilities. The high brilliance enables a broad range of techniques to be utilized which have high photon consumption. With soft X-ray spectroscopy the unoccupied (X-ray absorption) and occupied (X-ray emission) atomic and molecular orbitals are probed. A special case is resonant inelastic X-ray scattering (RIXS), where the excitation energy is set at a resonance.

Major chemical reactions and biological processes are occurring in liquid environments. Most life-important elements are light elements with an electronic configuration in the soft X-ray regime, which requires experimenting under vacuum conditions. Probing direct electronic structures of samples in a liquid phase is an experimental challenge. Two
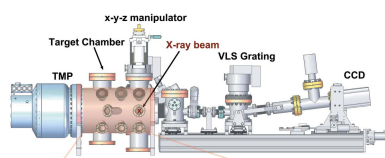
concepts have been introduced to probe liquid samples in a vacuum environment: the liquid cell and liquid jet (Yang & Kirz, 1987; Faubel *et al.*, 1988). When using a liquid cell the sample is isolated from the vacuum by thin X-ray transparent windows, *e.g.* made from Si_3N_4. However, the windows may interact with the sample. Despite the very small window thickness, absorption of the incoming and outgoing radiation cannot be avoided. This results in photon losses and longer data acquisition times. An advantage of this method is the small sample volume needed to perform the experiment. This can also be a disadvantage though, as radiation damage may occur. The latter can be avoided using the liquid jet. No windows are needed. The sample is refreshed with a repetition rate up to several MHz, depending on the flow rate, nozzle size and X-ray spot size. Yet, there is a high consumption of the compound. This is a major disadvantage when using very precious samples.

For detection of X-ray fluorescence an energy-dispersive detector is needed. The first pioneering work used a Rowland-circle-based grating spectrometer to detect soft X-rays (Callcott *et al.*, 1986; Nordgren *et al.*, 1989). The Rowland-circle-based X-ray spectrometer offers the possibility to easily increase the energy resolution by detecting higher orders of diffraction at the cost of decreasing detection efficiency. In recent years more spectrometers have been used based on the variable line spacing (VLS) design (Ghiringhelli *et al.*, 2006; Harada *et al.*, 2012; Chiuzbăian *et al.*, 2014; Yin *et al.*, 2015). Advantages are the reduced astigmatism and the focal plane geometry, allowing detectors to be utilized in normal incidence. Therefore, this leads to a larger energy range at one detector position. Currently, there exist a variety of RIXS setups for studying liquid samples (Blum *et al.*, 2009; Lange *et al.*, 2010; Tokushima *et al.*, 2008; Kunnus *et al.*, 2012).

In this work we present the novel experimental station, ChemRIXS, for chemical studies of liquid and solid samples utilizing RIXS. This new setup combines for the first time liquid jet technology with a soft X-ray spectrometer based on the VLS design. The advantages of windowless liquid samples in a vacuum coupled with a large energy detection range at sufficient energy resolution enable the investigation of the electronic configuration of biochemical processes in their natural environment. The setup is also equipped with a re-cycling device to reduce high sample consumption of the liquid jet technology.

In the following the details of the experimental endstation are described. In section 3, results from liquid and solid samples are presented. Very often, chemical analysis requires clear separation of superposing signals of complex systems. In order to emphasize such complexity in real-life samples, results from a mixture of relevant solvents in liquid phase and from samples with complex calgonite structures (solid) are presented.

2. Experimental setup

The endstation consists of a target chamber, the sample delivery system and a soft X-ray spectrometer based on the VLS principle (Yin *et al.*, 2015). The VLS spectrometer is a flexible unit that can also be installed on other target chambers of existing setups. A target holder is available for the liquid jet as well as for solid samples. As solid samples do not present challenges for the vacuum conditions, we concentrate on describing how the vacuum conditions are met when using the liquid jet. The main challenge is to fulfil the vacuum conditions of the beamline and the spectrometer. When we describe the setup we use the z-axis for the height; x is the direction of the interacting synchrotron beam and y is perpendicular to the synchrotron radiation beam. The layout of the setup and its dimensions are illustrated in Fig. 1. The target chamber is made from a 250 mm tube. The central axis of the tube is aligned to y. One end of the tube is terminated by a DN250CF for pumping with a turbo-molecular pump (TMP) at a pumping speed of $1900\,l\,s^{-1}$ (N_2), the other by a DN100CF flange for attaching the detection device, in our case the VLS spectrometer.

On the top and bottom are DN100CF flanges. These are needed for an x-y-z manipulator and a liquid-nitrogen-cooled trap or the recycling system on the opposite side. Around the sample positions are eight DN40CF flanges for installing
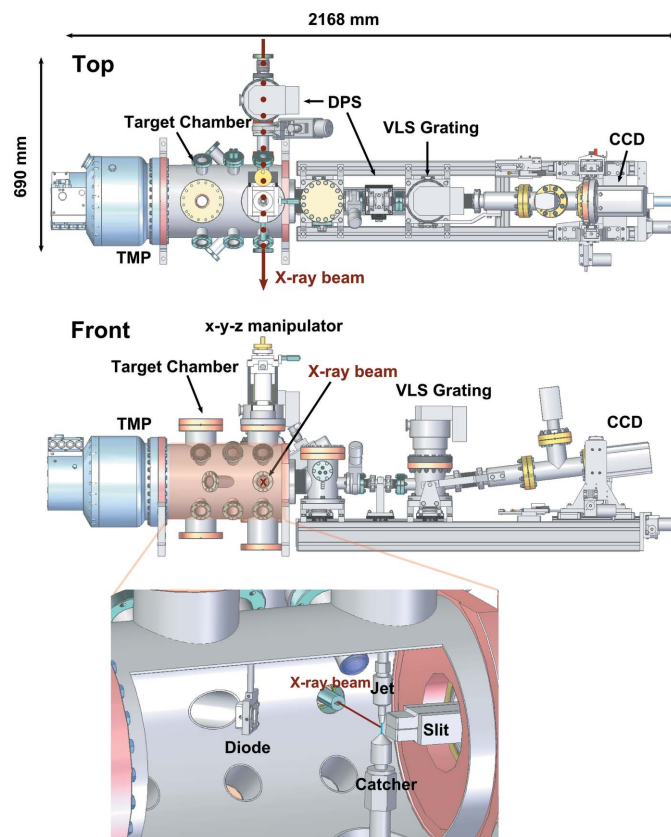

Figure 1
Top and front views of the setup are shown in the upper and middle tiers, respectively. The soft X-ray spectrometer is connected on the right-hand side of the target chamber. The TMP is connected on the left-hand side. One differential pumping stage (DPS) is placed between the outgoing flange of the beamline and the entrance flange of the target chamber. The second DPS is introduced between the target chamber and VLS grating chamber. The total length in this configuration is 690 mm. The enlargement at the bottom shows the setup with a running jet.

devices such as a photodiode to find the superposition of the incoming X-ray beam and liquid jet and a microscope to monitor the state of the sample. One challenge is to fulfil the ultrahigh-vacuum (UHV) conditions of the beamline which usually requires a vacuum of better than 10^{-8} mbar. The pressure in the main chamber depends on the nozzle size and the sample. Using a running jet with aqueous solutions, the vacuum is typically in the order of 10^{-4} mbar. The setup uses two differential pumping stages (DPSs) to fulfil the vacuum conditions. The first stage is attached directly to the target chamber *via* a narrow tube of length 5 cm with an elliptical cross section of 8 mm width and height of 4 mm. Together with a TMP this allows a pressure difference of up to three orders of magnitude to be overcome. The second DPS is a combination of a plate with a 10 mm hole and a TMP which overcomes an additional order of magnitude and fulfils the UHV conditions of the beamline. An HPLC pump delivers the liquid sample through the nozzle into the chamber. The small nozzle aperture and fast flow prevent freezing of the liquid due to evaporative cooling.

Shortly below the nozzle opening is the laminar flow of the sample. Depending on the sample, flow rate and nozzle size, the laminar flow can reach up to several millimetres. After the laminar range the liquid breaks up into droplets (Faubel *et al.*, 1988).

Besides probing the sample in a real liquid environment in a vacuum, the liquid jet offers a continuously refreshed sample and therefore prevents radiation damage, *i.e.* with a flow rate of 1 ml min^{-1} for a 20 μm nozzle and a beam spot size of 10 μm, a repetition rate >5 MHz can be reached. A 10 μm X-ray spot size is available at P04 at PETRA III (Viefhaus *et al.*, 2013). A mixing device allows switching between different samples without breaking the vacuum and opening the setup. A recycling system can be installed so that precious samples can be reused. This system consists of a conical formed catcher with a 100 μm hole on top and a membrane pump for pumping the sample out of the catcher of the vacuum system into a collecting tank. To avoid ice formation while hitting the catcher with aqueous solution, this part can be heated. The whole catcher system is on an *x-y-z* manipulator to align the recycling system (Charvat *et al.*, 2004). Tests show that the sample consumption can be limited to around 40 ml for a running experiment of 24 h. Therefore, the sample can be reused and precious samples can be studied in small amounts. The time after interaction with the X-ray beam and recycling must be larger than the relaxations time of the system to avoid radiation damage, otherwise artefacts might influence the true signal.

A grazing-incident VLS-design-based soft X-ray spectrometer is used to detect the X-ray fluorescence after core excitation. To reach the optimum performance of the spectrometer the geometrical conditions must be met as precisely as possible; one requirement is a small source size. The spectrometer is equipped with a slit system with slit sizes ranging from 100 μm down to 1 μm in micrometre steps. Since the liquid jet has a small diameter, in the 10–25 μm range, a small source size can be realised without using the slit system which
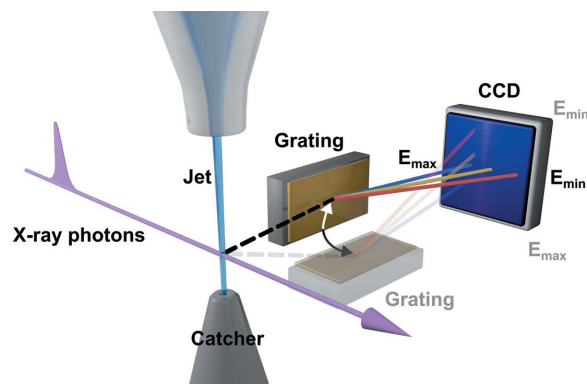

Figure 2
Geometrical layout for soft X-ray detection. The VLS grating focuses the incoming X-rays onto the focal plane which is perpendicular to the grating surface. The VLS spectrometer can be installed with the grating perpendicular (grey) or parallel (black) to the liquid jet.

is also ideal for detection efficiency. According to the focal simulation, derivation of the optimal incident angle leads to large discrepancies in the source–detector distance for different energies, while ray-tracing simulations show that small deviations in the source–grating distance are negligible. Ideally, the focal plane is correct at one distance for the whole energy range.

The spectrometer is equipped with an ANDOR iKon L CCD detector with 2048×2018 pixels with each having a pixel size of 13.5 μm resulting in a total detection area of 27.6 mm $\times$ 27.6 mm. Owing to charge spreading, the effective pixel size is around 27 μm (Ghiringhelli *et al.*, 2006). During the measurements the CCD was cooled down to 193 K to reduce thermal noise. Another advantage of this spectrometer is that it can be operated under relatively high vacuum conditions. It is implemented with a DPS between the slit system and the grating which can overcome about two orders of magnitude without losing photon intensity. Fig. 2 shows a schematic layout. A detailed description of the spectrometer can be found elsewhere (Yin *et al.*, 2015).

An additional feature is that the spectrometer can be installed either with the grating in the plane of the synchrotron beam or in the perpendicular direction to improve the detection efficiency depending on the dimensions of the focal spot size on the sample (see Fig. 2).

The apparatus is also equipped with a photodiode for performing X-ray absorption measurements in total fluorescence yield (see Fig. 1).

The total dimensions of the setup are 2168 mm in length and 690 mm in width. The width from the DPS flange to the middle of the target chamber is 511 mm and can be reduced to 430 mm. This compact design allows the experimental setup to be deployed at different synchrotron radiation and free-electron laser facilities. In the following section, we present experimental results from liquid and solid samples.

3. Results

The results of experiments using liquid and solid samples are presented to illustrate the capability of the setup. As samples,

Figure 4
Acetonitrile emission signal from the 2e and 7a1 orbital into the 1s of nitrogen at 391.4 eV and 392.6 eV, respectively. The emission signal at 400 eV is the elastic scattering from the incoming beam. The X-ray absorption spectrum of acentonitrile, from which the excitation energy is chosen, is shown in the inset.

important organic solvents have been chosen. The beam spot was 300 µm × 10 µm for the liquid sample and 1 mm × 1 mm for the solid sample, to reduce radiation damage. For the liquid experiment a ∼25 µm nozzle was used. The beamline resolution was set at ∼2 eV.

3.1. Application of a liquid sample

In order to demonstrate the large energy detection range, Fig. 3 shows the X-ray emission signal for a 1:1 acetonitrile–ethanol mixture. It is probed using an excitation energy of 540 eV in the liquid phase at an optimal detector position for the nitrogen emission signal. The total exposure time was set to 5 min with a ∼300 µm × 10 µm beam spot. X-ray emission lines of oxygen in first and second order and nitrogen and carbon in first order are observed. In total, with this configuration an energy range of ∼300 eV was covered.

The strongest signal derives from oxygen in first order followed by the second order and carbon and nitrogen signals. The nitrogen and carbon emission lines are the weakest. At 540 eV excitation energy the photons are absorbed mostly by the oxygen in ethanol which explains the strong line of oxygen in first and second order. The number of carbon atoms is
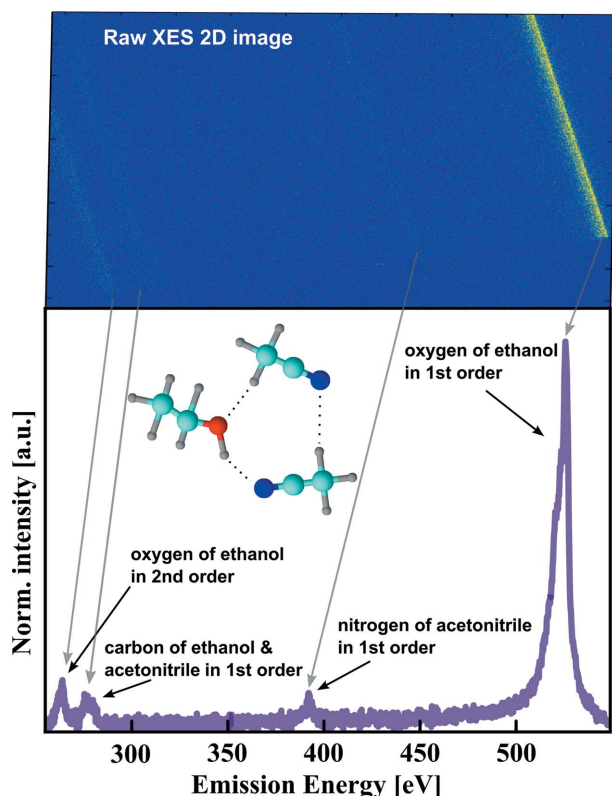

Figure 3
Wide-energy spectrum for investigation of complex solvents. The top tier shows the raw XE spectrum of the ethanol–acetonitrile mixture. The bottom tier shows the emission lines of oxygen in first and second order as well as of nitrogen from acetonitrile and carbon from both. The excitation energy was set at 540 eV which is mostly absorbed by the core electron of oxygen in ethanol. The inset shows a possible ethanol–acetonitrile configuration. The elements are colour coded in red (oxygen), grey (hydrogen), blue (nitrogen) and cyan (carbon) while the dotted lines represent hydrogen bonds.
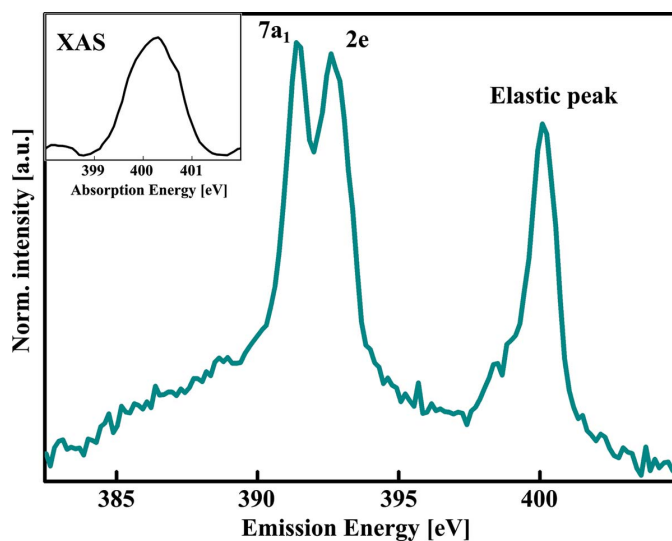
higher than the number of nitrogen atoms but the higher cross sections of the nitrogen 1s electrons compensate the lower signal of this element.

Compared with previous measurements at similar energy resolution (Dierker et al., 2013) the energy range is extended by a factor of about four. This offers the possibility to measure the characteristic emission lines of more than one element at the same time. In this case the three elements carbon, nitrogen and oxygen are shown in Fig. 3.

In order to show the possible energy resolution, the excitation energy is tuned to the nitrogen K-edge. Fig. 4 shows the X-ray emission (XE) spectrum of nitrogen for an excitation energy of 400 eV which is the resonance of the core electron of nitrogen. The emission signal of ethanol vanished as expected due to the low absorption cross section of oxygen.

The spectrum shows the emission signal from the 7a1 and 2e orbitals after core excitation at the nitrogen K-edge. The signal agrees with previously reported results (Dierker et al., 2013). The excitation energy at 400 eV is determined according to the X-ray absorption spectrum detected in total fluorescence yield mode using a diode. A practical feature of P04 is its 'on the fly' mode which allows X-ray absorption spectra to be recorded relatively quickly (Viefhaus et al., 2013).

3.2. Application to a solid sample

Fig. 5 shows the X-ray emission spectrum of an epitaxial $Pr_{0.7}Ca_{0.3}MnO_3$ (PCMO) thin film excited on the manganese L-edge. To reduce the risk of radiation damage the X-ray beam spot was enlarged to ∼1 mm × 1 mm, which decreased the energy density on the sample at the cost of lower detection efficiency and lower energy resolution. The X-ray emission
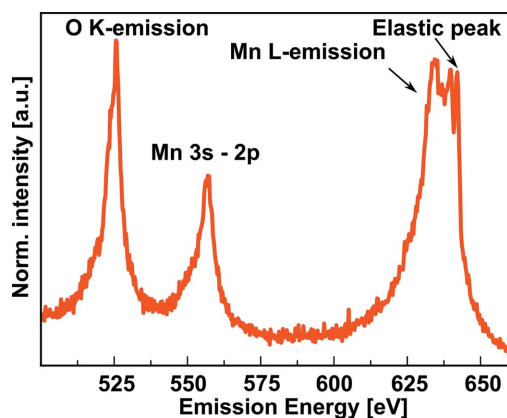
Figure 5
X-ray emission spectrum of a $Pr_{0.7}Ca_{0.3}MnO_3$ thin film. Only the part with emission signals is presented. Due to the advantage of the wide energy range, the emission lines of oxygen and manganese are recorded without changing the detector position.

spectrum shows the oxygen K-emission and the manganese L-emission lines.

A 300 nm-thick film has been deposited by reactive ion beam sputtering on 200 nm of sputtered Pt on MgO single-crystal substrate (Mildner *et al.*, 2015). PCMO shows strong electron–electron and electron–lattice correlations. The band structure near the Fermi energy comprises strongly hybridized bands containing Mn $3d$ and O $2p$ states. The emission spectrum shows the wide range of relaxations from Mn $3s$ to Mn $2p$ (about 560 eV) as well as from the O $2p$–Mn $3d$ band to O $1s$ (O K at about 525 eV) and to Mn $2p$ ($L_{3/2}$ at about 640–660 eV). Elastic scattering of the beam is located at 642 eV.

4. Conclusion

In this work we present a novel endstation for RIXS studies of liquid and solid samples in the soft X-ray regime. ChemRIXS combines liquid jet technology with a soft X-ray VLS spectrometer and offers the advantages of real liquid samples under vacuum and the easy use of a soft X-ray spectrometer based on the VLS principle. ChemRIXS is also equipped with a photodiode to detect XAS spectra in total fluorescence yield mode. The first experimental results of liquid and solid samples showed a working setup with sufficient resolution power. Compared with similar setups the spectrometer can cover an energy range of approximately 300 eV which is almost four times wider compared with the Rowland-circle-based spectrometer with comparable energy resolution. This enables measurement of various element edges using one-shot procedures, which is particularly interesting as a portable analysis endstation for investigation of chemical reactions at free-electron laser facilities.

References

Ament, L., van Veenendaal, M., Devereaux, T., Hill, J. & van den Brink, J. (2011). *Rev. Mod. Phys.* **83**, 705–767.
Blum, M., Weinhardt, L., Fuchs, O., Bär, M., Zhang, Y., Weigand, M., Krause, S., Pookpanratana, S., Hofmann, T., Yang, W., Denlinger, J. D., Umbach, E. & Heske, C. (2009). *Rev. Sci. Instrum.* **80**, 123102.
Callcott, T. A., Tsang, K. L., Zhang, C. H., Ederer, D. L. & Arakawa, E. T. (1986). *Rev. Sci. Instrum.* **57**, 2680.
Charvat, A., Lugovoj, E., Faubel, M. & Abel, B. (2004). *Rev. Sci. Instrum.* **75**, 1209.
Chiuzbăian, S. G., Hague, C. F., Avila, A., Delaunay, R., Jaouen, N., Sacchi, M., Polack, F., Thomasset, M., Lagarde, B., Nicolaou, A., Brignolo, S., Baumier, C., Lüning, J. & Mariot, J.-M. (2014). *Rev. Sci. Instrum.* **85**, 043108.
Dierker, B., Suljoti, E., Atak, K., Lange, K. M., Engel, N., Golnak, R., Dantz, M., Hodeck, K., Khan, M., Kosugi, N. & Aziz, E. F. (2013). *New J. Phys.* **15**, 093025.
Faubel, M., Schlemmer, S. & Toennies, J. P. (1988). *Z. Phys. D*, **10**, 269–277.
Ghiringhelli, G., Piazzalunga, A., Dallera, C., Trezzi, G., Braicovich, L., Schmitt, T., Strocov, V. N., Betemps, R., Patthey, L., Wang, X. & Grioni, M. (2006). *Rev. Sci. Instrum.* **77**, 113108.
Harada, Y., Kobayashi, M., Niwa, H., Senba, Y., Ohashi, H., Tokushima, T., Horikawa, Y., Shin, S. & Oshima, M. (2012). *Rev. Sci. Instrum.* **83**, 013116.
Kotani, A. & Shin, S. (2001). *Rev. Mod. Phys.* **73**, 203–246.
Kunnus, K., Rajkovic, I., Schreck, S., Quevedo, W., Eckert, S., Beye, M., Suljoti, E., Weniger, C., Kalus, C., Grübel, S., Scholz, M., Nordlund, D., Zhang, W., Hartsock, R. W., Gaffney, K. J., Schlotter, W. F., Turner, J. J., Kennedy, B., Hennies, F., Techert, S., Wernet, P. & Föhlisch, A. (2012). *Rev. Sci. Instrum.* **83**, 123109.
Lange, K. M., Könnecke, R., Ghadimi, S., Golnak, R., Soldatov, M. A., Hodeck, K. F., Soldatov, A. & Aziz, E. F. (2010). *Chem. Phys.* **377**, 1–5.
Mildner, S., Hoffmann, J., Blöchl, P. E., Techert, S. & Jooss, C. (2015). *Phys. Rev. B*, **92**, 035145.
Nordgren, J., Bray, G., Cramm, S., Nyholm, R., Rubensson, J.-E. & Wassdahl, N. (1989). *Rev. Sci. Instrum.* **60**, 1690.
Tokushima, T., Harada, Y., Takahashi, O., Senba, Y., Ohashi, H., Pettersson, L. G. M., Nilsson, A. & Shin, S. (2008). *Chem. Phys. Lett.* **460**, 387–400.
Viefhaus, J., Scholz, F., Deinert, S., Glaser, L., Ilchen, M., Seltmann, J., Walter, P. & Siewert, F. (2013). *Nucl. Instrum. Methods Phys. Res. A*, **710**, 151–154.
Yang, B. X. & Kirz, J. (1987). *Phys. Rev. B*, **36**, 1361–1364.
Yin, Z., Peters, H. B., Hahn, U., Agåker, M., Hage, A., Reininger, R., Siewert, F., Nordgren, J., Viefhaus, J. & Techert, S. (2015). *Rev. Sci. Instrum.* **86**, 093109.